A Stoichiometric Nano-$LiMn_2O_4$ Spinel Electrode Exhibiting High Power and Stable Cycling

Kuthanapillil M. Shaju and Peter G. Bruce*

EaStChem, School of Chemistry, University of St. Andrews, St. Andrews, KY16 9ST, U.K.

Received April 23, 2008. Revised Manuscript Received June 19, 2008

Stoichiometric $LiMn_2O_4$ has been synthesized using a one-pot resorcinol−formaldehyde route. The resulting material is composed of nanoparticles fused together, thus forming a porous morphology. The material when used as a cathode in a lithium battery exhibits, at 30 °C, an initial capacity of 131 mA·h g^{-1} retaining a capacity of 118 mA·h g^{-1} after 200 cycles (99.95% capacity retention per cycle) and at 50 °C an initial capacity of 132 mA·h g^{-1} retaining 110 mA·h g^{-1} after 200 cycles (99.92% capacity retention per cycle) all at a rate of *C*/2 (where $1C = 148$ mA g^{-1}), with no evidence of structural degradation. Rate capability is demonstrated by retention of 90% of the capacity at a rate of 40*C* compared with the capacity at *C*/5 rate. Cycling at a rate of 10*C* is associated with nearly 100% power retention after 1000 cycles (initial value of 5840 W kg^{-1} (of $LiMn_2O_4$) dropping to 5828 W kg^{-1} after 1000 cycles). Differences in the capacity retention on cycling between the material reported here and conventionally synthesized bulk $LiMn_2O_4$ or nanoparticle $LiMn_2O_4$ synthesized by a different sol−gel route also yielding interconnected nanoparticles are reflected in superior structural stability, lower Mn dissolution, and relatively invariant ac impedance of our nano-$LiMn_2O_4$. Such results suggest that the material prepared using the resorcinol−formaldehyde route may possess a stabilized surface that inhibits dissolution.

Introduction

Future rechargeable lithium batteries require lithium intercalation cathodes that combine low cost, low toxicity, and high safety with high rates of intercalation/deintercalation. The lithium intercalation compounds $LiFePO_4$ olivine[1] and $LiMn_2O_4$[2−10] spinel have received particular attention in this regard. The latter has been studied as an intercalation electrode for many years and exhibits a potential of 4 V versus Li^+ (1 M)/Li when cycled over the composition range of $Li_xMn_2O_4$, $0 < x < 1$.[2−10] Early work soon identified that stoichiometric $LiMn_2O_4$ shows considerable capacity fading on cycling, associated with structural degradation, and poor rate performance.[3−9] As a result, attention turned to nonstoichiometric spinels such as $Li_{1.05}Mn_{1.95}O_4$, which demonstrate better cycling stability despite lower theoretical and practical capacities due to a Mn valence >3.5.[3−10] These materials failed to show sufficient stability on cycling at elevated temperatures (~50 °C) resulting in the study of even less stoichiometric compositions, i.e., more Li-rich further compromising capacity, doping with foreign ions (e.g., F^-, transition metals), application of coatings (e.g., ZnO, $LiCoO_2$), or utilization of electrolyte additives or different electrolytes.[5−14]

Here we show that stoichiometric $LiMn_2O_4$ may be synthesized by a one-pot resorcinol−formaldehyde route, resulting in a material composed of nanoparticles fused together, thus forming a porous morphology. The material, hereafter referred to as nano-$LiMn_2O_4$, exhibits good rate performance, as might be expected due to its nanomorphology, but also excellent capacity retention on cycling at 30

* Corresponding author. E-mail: P.G.Bruce@st-andrews.ac.uk.

(1) Padhi, A. K.; Nanjundaswamy, K. S.; Goodenough, J. B. *J. Electrochem. Soc.* **1997**, *144*, 1188.
(2) (a) a Thackeray, M. M.; Johnson, P. J.; Depicciotto, L. A.; Bruce, P. G.; Goodenough, J. B. *Mater. Res. Bull.* **1984**, *19*, 179. (b) Thackeray, M. M. *Prog. Solid State Chem.* **1997**, *25*, 1. (c) Tarascon, J. M.; Guyomard, D. *J. Electrochem. Soc.* **1991**, *138*, 2864.
(3) (a) a Pasquier, A. D.; Blyr, A.; Courjal, P.; Larcher, D.; Amatucci, G.; Gerand, B.; Tarascon, J. M. *J. Electrochem. Soc.* **1999**, *146*, 428. (b) Amatucci, G.; Tarascon, J. M. *J. Electrochem. Soc.* **2002**, *149*, K31. (c) Huang, H.; Vincent, C. A.; Bruce, P. G. *J. Electrochem. Soc.* **1999**, *146*, 3649. (d) Shin, Y.; Manthiram, A. *J. Electrochem. Soc.* **2004**, *151*, A204.
(4) (a) Cho, J.; Thackeray, M. M. *J. Electrochem. Soc.* **1999**, *146*, 3577. (b) Xia, Y.; Sakai, T.; Fujieda, T.; Yang, X. Q.; Sun, X.; Ma, Z. F.; McBreen, J.; Yoshio, M. *J. Electrochem. Soc.* **2001**, *148*, A723. (c) Takada, T.; Hayakawa, H.; Enoki, H.; Akiba, E.; Slegr, H.; Davidson, I.; Murray, J. *J. Power Sources* **1999**, *81*−*82*, 505. (d) Thackeray, M. M.; Yang, S. H.; Kahaian, A. J.; Kepler, K. D.; Skinner, E.; Vaughey, J. T.; Hackney, S. A. *Electrochem. Solid-State Lett.* **1998**, *1*, 7.
(5) Xia, Y.; Zhou, Y.; Yoshio, M. *J. Electrochem. Soc.* **1997**, *144*, 2593.
(6) Amatucci, G. G.; Pereira, N.; Zheng, T.; Tarascon, J. M. *J. Electrochem. Soc.* **2001**, *148*, A171.
(7) Larcher, D.; Gerand, B.; Tarascon, J. M. *J. Solid State Electrochem.* **1998**, *2*, 137.
(8) Shin, Y.; Manthiram, A. *Chem. Mater.* **2003**, *15*, 2954.
(9) Kannan, A. M.; Manthiram, A. *Electrochem. Solid-State Lett.* **2002**, *5*, A167.
(10) (a) Song, D.; Ikuta, H.; Uchida, T.; Wakihara, M. *Solid State Ionics* **1999**, *117*, 151. (b) Shaju, K. M.; Subba Rao, G. V.; Chowdari, B. V. R. *Solid State Ionics* **2002**, *148*, 343. (c) Okada, M.; Lee, Y.-S.; Yoshio, M. *J. Power Sources* **2000**, *90*, 196.
(11) Sun, Y. K.; Hong, K. J.; Prakash, J. *J. Electrochem. Soc.* **2003**, *150*, A970.
(12) Liu, H.; Cheng, C.; Zongqiuhu; Zhang, K. *Mater. Chem. Phys.* **2007**, *101*, 276.
(13) Li, C.; Zhang, H. P.; Fu, L. J.; Liu, H.; Wu, Y. P.; Rahm, E.; Holze, R.; Wu, H. Q. *Electrochim. Acta* **2006**, *51*, 3872.
(14) (a) Chen, Z.; Lu, W. Q.; Liu, J.; Amine, K. *Electrochim. Acta* **2006**, *51*, 3322. (b) Zhang, S. S.; Xu, K.; Jow, T. R. *J. Power Sources* **2006**, *154*, 276. (c) Yu, B. T.; Qiu, W. H.; Li, F. S.; Cheng, L. *J. Power Sources* **2007**, *166*, 499.

10.1021/cm8010925 CCC: $40.75
Published on Web 08/09/2008

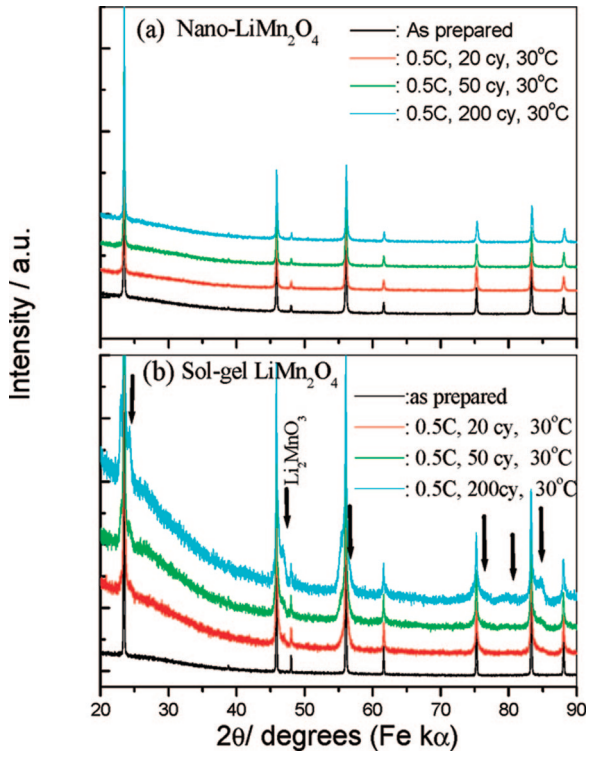

Figure 1. Powder X-ray diffraction patterns of the as-prepared samples and at the end of discharge after cycling at 30 °C to 20, 50, and 200 cycles (74 mA g^{-1} (*C*/2) 3.5−4.3 V) for (a) nano- and (b) sol−gel $LiMn_2O_4$. Vertical arrows indicate peak positions for Li_2MnO_3.

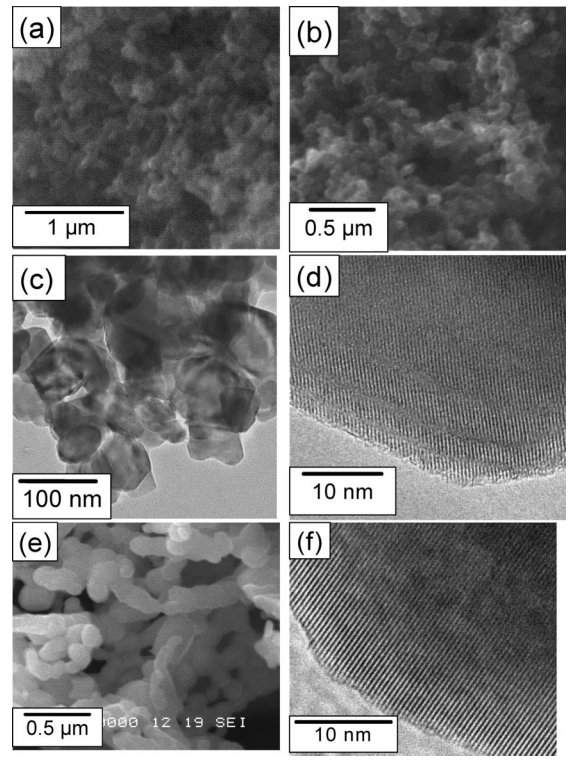

Figure 2. (a) SEM of as-prepared nano-$LiMn_2O_4$, (b) SEM of a nano-$LiMn_2O_4$ electrode after 50 cycles between 3.5 and 4.3 V at 74 mA g^{-1}, (c and d) TEM of as-prepared nano-$LiMn_2O_4$, (e) SEM of as-prepared sol−gel $LiMn_2O_4$, and (f) TEM of as-prepared sol−gel $LiMn_2O_4$.

and 50 °C, no structural degradation, and low Mn dissolution. Such behavior is in contrast to that generally observed for stoichiometric $LiMn_2O_4$ prepared by other methods, whether composed of nanometer or micrometer particles.

Experimental Section

Synthesis of nano-$LiMn_2O_4$ was carried out by dissolving $LiCH_3COO\cdot 2H_2O$ and $Mn(CH_3COO)_2\cdot 4H_2O$ (Fluka; ≥99%) in quantities corresponding to 0.02 mol of stoichiometric $LiMn_2O_4$ in 100 mL of water containing 0.1 mol of resorcinol (Fluka 99%) and 0.15 mol of formaldehyde (Fluka 36.5% in water, methanol-stabilized). The mixture was then heated at 60 °C until viscous, then 90 °C for 24 h, followed by calcination at 750 °C for 12 h to obtain nano-$LiMn_2O_4$. All procedures were carried out in air. $LiMn_2O_4$ powders were also prepared by a sol−gel method following a previously published procedure with cation ratio of Li/Mn = 1.0:2.0.[11]

Powder X-ray diffraction (PXRD) was carried out using a Stoe STADI/P diffractometer operating in transmission mode using an Fe source. Lattice parameters were obtained from PXRD data by Rietveld refinement using FullProf. Chemical analysis was carried out by inductively coupled plasma atomic emission spectrometry (ICP-AES) and was performed at the CNRS facility in Vernaison (France). Morphological studies were conducted using a Jeol JSM-5600 scanning electron microscope (SEM) and Jeol JEM-2011 transmission electron microscope (TEM). Surface area measurements were obtained using the Brunauer, Emmett, and Teller (BET) method employing a Micromeritics Gemini 23670 instrument and nitrogen gas. The oxidation state of manganese in $LiMn_2O_4$ was determined by the iodometric titration method as described previously.[30] The carbon content was determined by CHN analysis (CE Instrument, EA 1110 CHNS).

To evaluate electrochemical performance, coin cells (NRC 2325) were assembled employing a composite electrode (active material, Kynar 2801 (a copolymer based on PVDF) and super S carbon, in the weight ratios of 76:12:12 with typical active material loading of 6−7 mg cm^{-2}) with lithium metal as the counter electrode and LP30 (Merck; 1 M $LiPF_6$ in 1:1 v/v ethylene carbonate/dimethylene carbonate (EC/DMC)) as electrolyte. More details may be found elsewhere.[15] Electrochemical measurements at 30 and 50 (±1) °C were carried out using a Maccor series 4200 battery cycler. The ac impedance measurements were conducted on three-electrode cells with lithium metal as the counter and reference electrodes and LP30 as electrolyte. Data were collected using a Solartron 1255 frequency response analyzer coupled with Solartron 1286 electrochemical interface. A perturbation voltage of 5 mV and frequency range from 50 kHz to 10 mHz were employed.

Results and Discussion

The synthesis of nano-$LiMn_2O_4$ by the resorcinol−formaldehyde route is described in the Experimental Section. The PXRD pattern for this material is shown in Figure 1 and corresponds to a single-phase $LiMn_2O_4$ spinel with an a_0 lattice parameter, obtained by Rietveld refinement, of 8.237 Å, in excellent agreement with the value expected for stoichiometric $LiMn_2O_4$.[3,4,6] Chemical and oxidation state analysis confirmed the stoichiometric composition, within ±1%. The CHN analysis indicated that the carbon content was negligible, i.e., below the detection limit of the instrument. The morphology, Figure 2, is that of interconnected

(15) (a) Shaju, K. M.; Bruce, P. G. *Adv. Mater.* **2006**, *18*, 2330. (b) Shaju, K. M.; Bruce, P. G. *J. Power Sources* **2007**, *174*, 1201.

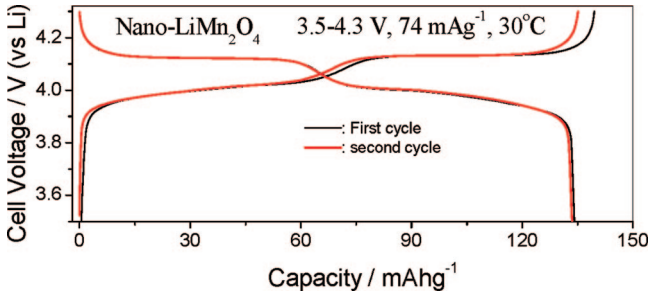

Figure 3. Charge and discharge voltage profiles for nano-$LiMn_2O_4$ at 74 mA g^{-1} (~0.4 mA cm^{-2}) between 3.5−4.3 V for the first and second cycles at 30 °C.

nanoparticles (50−100 nm) forming a porous morphology, with pores between 2−5 μm. This structure is preserved on fabricating composite electrodes and after cycling, Figure 2. The BET surface area determined from N_2 desorption is 14 m^2 g^{-1}. A similar morphology has been observed previously for $Li(Ni_{1/3}Co_{1/3}Mn_{1/3})O_2$ prepared using the resorcinol−formaldehyde route.[15] $LiMn_2O_4$ prepared by a different sol−gel route (described previously and in the Experimental Section), hereafter referred to as sol−gel $LiMn_2O_4$, also possesses an interconnected nanoparticle morphology. Although the particles are somewhat bigger, at around 200 nm, the surface area is similar, 13 m^2 g^{-1}, compared with nano-$LiMn_2O_4$, implying that in the latter case the particles are more tightly fused together. The morphology is also invariant on cycling (Figure 2e).

Nano-$LiMn_2O_4$was incorporated into a composite electrode, as described in the Experimental Section. Charge/discharge curves collected on cycling at a rate of *C*/2 (*C* = 148 mA g^{-1}) are shown in Figure 3 and exhibit the well-known pair of plateaus for stoichiometric $LiMn_2O_4$ centered around 4 V and separated by around 100 mV.[2−5] The variation of discharge capacity with cycle number, for up to 200 cycles, is shown in Figure 4 where it is compared with stoichiometric $LiMn_2O_4$ prepared by the other sol−gel method. All electrodes and cells were fabricated identically. The PXRD of sol−gel $LiMn_2O_4$ corresponds to stoichiometric spinel, a_0 = 8.239 Å. The initial capacity, at a discharge rate of *C*/2, for nano-$LiMn_2O_4$ is 131 mA·h g^{-1}, retaining a capacity of 118 mA·h g^{-1} after 200 cycles (99.95% retention per cycle). In comparison, the initial cycles of sol−gel $LiMn_2O_4$ exhibit a capacity of 133 mA·h g^{-1}, fading significantly on subsequent cycles, retaining 80 mA·h g^{-1} at the end of 200 cycles (99.80% retention per cycle). In accord with these results, PXRD data for sol−gel $LiMn_2O_4$ exhibits the structural degradation usually observed for stoichiometric $LiMn_2O_4$, whereas nano-$LiMn_2O_4$ exhibits no such degradation, as discussed latter, Figure 1. The behavior of nano-$LiMn_2O_4$ at elevated temperatures has also been investigated and is presented in Figure 4b. Capacity retention per cycle at a rate of *C*/2 is 99.92% and is again substantially better than sol−gel $LiMn_2O_4$, which exhibits a capacity retention of only 99.77% per cycle. The behavior of nano-$LiMn_2O_4$ at 30 and 50 °C is not only in sharp contrast to that of sol−gel $LiMn_2O_4$ with the same surface area but compares favorably with the widely

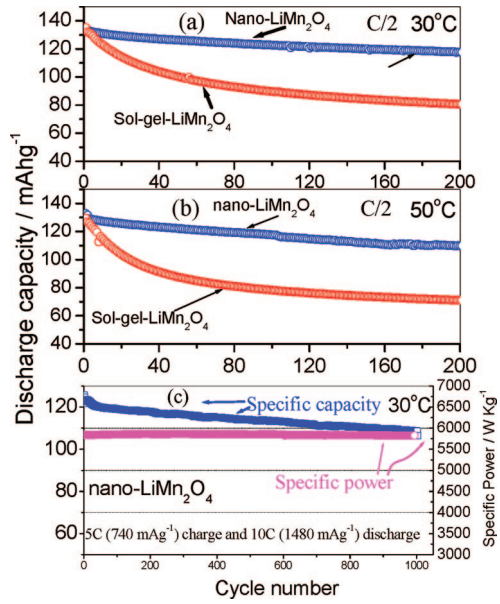

Figure 4. (a) Cycling performance for nano- and sol−gel $LiMn_2O_4$ at 30 °C, rate *C*/2 (74 mA g^{-1}, ~0.4 mA cm^{-2}), (b) as for (a) but at 50 °C, and (c) performance of nano-$LiMn_2O_4$ at a 10*C* discharge rate and 30 °C; capacity and corresponding specific power densities (calculated based on active mass) are shown up to 1000 cycles.

reported cycling performance of stoichiometric $LiMn_2O_4$ in general, whether composed of nanometer- or micrometer-sized particles, Table 1. In fact the capacity retention resembles more closely that of surface-coated or fluorinated $LiMn_2O_4$, Table 1.

The rate capability of nano-$LiMn_2O_4$ is presented in Figure 5. The rate capability is expressed as the capacity at a given discharge rate relative to that obtained at a rate of ~*C*/5. The rate performance of nano-$LiMn_2O_4$ is excellent, corresponding to 90% retention of capacity at 40*C* and 85% at 60*C* (8880 mA g^{-1}, discharge in 42 s). The performance of nano-$LiMn_2O_4$ exceeds that of sol−gel $LiMn_2O_4$ with the same surface area. The voltage profiles of nano-$LiMn_2O_4$ at different *C*-rates are shown in Figure 5b. The rate performance of nano-$LiMn_2O_4$ may be compared with data from the literature, Table 2, which confirms the good rate capability of nano-$LiMn_2O_4$.

To explore whether the good rate capability is retained on prolonged cycling, nano-$LiMn_2O_4$ has been cycled at a rate of 10*C* (1480 mA g^{-1}) for 1000 cycles, Figure 4c. The results show an initial capacity of 120 mA·h g^{-1}, retaining 109 mA·h g^{-1} after 1000 cycles. The specific power (based on the active mass of material) is also plotted in Figure 4c, and it shows no fade up to 1000 cycles. This is due an almost invariant average voltage of the cell on

(16) Kim, J. S.; Johnson, C. S.; Vaughey, J. T.; Hackney, S. A.; Walz, K. A.; Zeltner, W. A.; Anderson, M. A.; Thackeray, M. M. *J. Electrochem. Soc.* **2004**, *151*, A1755.
(17) Jiang, C. H.; Dou, S. X.; Liu, H. K.; Ichihara, M.; Zhou, H. S. *J. Power Sources* **2007**, *172*, 410.
(18) Zhang, Y.; Shin, H. C.; Dong, J.; Liu, M. *Solid State Ionics* **2004**, *171*, 25.
(19) Huang, S.; Wen, Z.; Yang, X.; Zhu, X.; Lin, B. *Electrochem. Solid-State Lett.* **2006**, *9*, A443.
(20) Luo, J.; Cheng, L.; Xia, Y. *Electrochem. Commun.* **2007**, *9*, 1404.
(21) Park, S. C.; Han, Y. S.; Kang, Y. S.; Lee, P. S.; Ahn, S.; Lee, H. M.; Lee, J. Y. *J. Electrochem. Soc.* **2001**, *148*, A680.

Table 1. Performance of Stoichiometric, Nonstoichiometric, and Surface-Coated Li−Mn−O Spinels from the Literature[a]

composition/description	*C*-rate (corresponding temperatures)	% capacity retention per cycle	refs
$LiMn_2O_4$	0.33, 0.2, 0.2 (25, 22, and 25 °C)	99.85, 99.75, 99.21	5, 6, 8
$LiMn_2O_4$	0.33, 0.2, 0.33 (50, 60, and 50 °C)	99.62, 99.59, 99.27	5, 9, 16
$LiMn_2O_4$	8, 0.5 (25 °C)	99.88, 99.5	17, 18
Ag/$LiMn_2O_4$ composite	4 (25 °C)	99.8	19
$Li_{1.05}Mn_{1.95}O_4$	0.2, 0.2, 1 (25 °C)	99.96, 99.81, 99.98	7, 8, 20
$Li_{1.05}Mn_{1.95}O_4$	0.2, 0.2 (55 °C)	99.76, 99.85	6, 7
$LiAl_{0.2}Mn_{1.8}O_{4-\delta}F_{0.5}$	0.2 (55 °C)	99.94	6
$LiCoO_2$-modified $LiMn_2O_4$	0.5, 2 (25 °C)	99.97, 99.96	9
ZnO-coated $LiMn_2O_4$	0.33 (55 °C)	99.94	11, 12

[a] Percent capacities and refs in columns 3 and 4, respectively, correspond to the *C*-rates given in column 2.

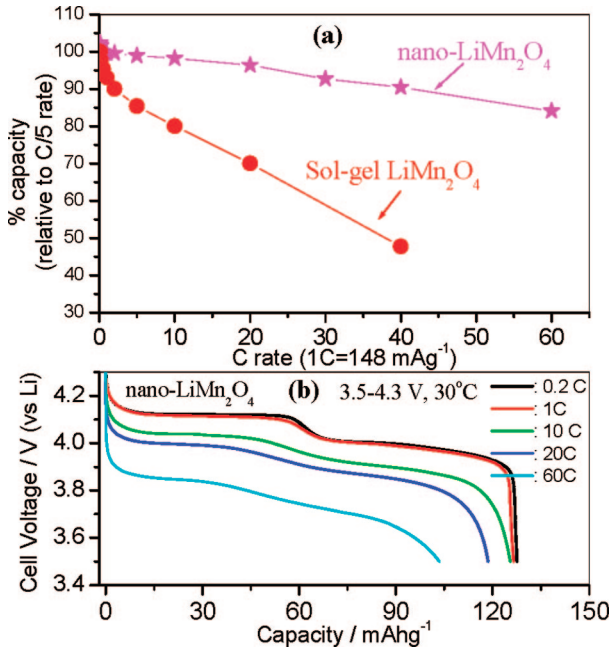

Figure 5. (a) Rate performance of nano-$LiMn_2O_4$ compared with sol−gel $LiMn_2O_4$. The rate capability is expressed as the percentage of the capacity obtained at a specific discharge rate compared to that obtained at a low rate of *C*/5 (30 mA g^{-1}; ∼0.15 mA cm^{-2}). (b) The discharge voltage profile for nano-$LiMn_2O_4$ at different *C*-rates.

Table 2. Rate Performance for Li−Mn−O Spinels (Stoichiometric, Nonstoichiometric, as Well as Surface-Coated) from the Literature[a]

composition/specification	*C*-rate	% capacity retention[b]	refs
$LiMn_2O_4$	4, 10, 20	47, 57, 46	8, 18, 21
$Li_{1.05}Mn_{1.95}O_4$	4	82	8
$Li_{1.09}Mn_{1.91}O_4$	20	80	22
$Li_{1.05}Mn_{1.95}O_4$[c]	15	70	20
$LiMn_{1.85}Ni_{0.075}Li_{0.075}O_4$	10, 20	84, 57	8
$Li_{1.04}Mg_{0.045}Mn_{1.92}O_4$	10	83	23
6.3 wt % Ag−$LiMn_2O_4$ composite	10	94	19
alumina-coated thin film	45	79	24
$LiCoO_2$ (7%)-coated $LiMn_2O_4$	20	83	21

[a] The electrode formulation, thickness, active material loading, and cell fabrication used in different laboratories may vary, and hence, comparisons may only be approximate. [b] Capacity retention compared with capacity at ∼*C*/5 rate. [c] $Li_{1.05}Mn_{1.95}O_4$ hollow nanospheres.

cycling. It may be noted that, at 20*C*, the specific power is >11 000 W kg^{-1} for nearly 2 min, which compares favorably with the value of 8000 W kg^{-1} for about 100 s reported previously.[22]

To determine whether the volumetric energy density of nano-$LiMn_2O_4$ is significantly compromised because of the small particle size/porous morphology, we have evaluated the volumetric energy density using the actual volume of the electrode measured directly, following the procedure described earlier.[15] The volumetric energy density (based on total electrode volume including conducting carbon and binder) is 785 W·h L^{-1} at 0.1*C*, which is similar to that observed for spinel with micrometer-sized particles at comparably low rates. This may be due to the carbon and the binder occupying some of the pore volume thus negating the effect of porosity on the volumetric energy density. On increasing the rate, a volumetric energy density of 750 W·h L^{-1} is retained at 20*C*.

The significant capacity fading normally observed for stoichiometric $LiMn_2O_4$ has been attributed to several causes including, Mn^{3+} disproportionation to Mn^{2+} and Mn^{4+}, followed by Mn^{2+} dissolution in the electrolyte, the onset of the Jahn−Teller (J−T) distortion near the end of discharge, or the small difference in the lattice parameters between Mn_2O_4 and $Li_{0.5}Mn_2O_4$, with dissolution being the most frequently cited cause.[3−9,11,25] Such disproportionation and dissolution is associated with degradation of the $LiMn_2O_4$ spinel structure, on cycling.[4,11,25] As dissolution proceeds and the proportion of Mn^{4+} in the remaining spinel increases, Li_2MnO_3 is formed, as seen in powder diffraction patters of cycled materials.[4,11,25] PXRD data for nano-$LiMn_2O_4$ and sol−gel $LiMn_2O_4$, in the discharged state, after various numbers of charge/discharge cycles, are shown in Figure 1. Structural degradation of sol−gel $LiMn_2O_4$ is evident in Figure 1. The additional peaks that appear on cycling are identical to those observed previously for cycled $LiMn_2O_4$ and include the major peaks from Li_2MnO_3.[4,11,25] These diffraction data are in sharp contrast to those for nano-$LiMn_2O_4$ after cycling under identical conditions, Figure 1. The PXRD for nano-$LiMn_2O_4$ demonstrate excellent structural stability on cycling, in good accord with the high degree of capacity retention, Figure 4.

The structural stability and good capacity retention for stoichiometric nano-$LiMn_2O_4$ suggest a low level of Mn dissolution in the electrolyte. The manganese solubility in LP30 (1 M $LiPF_6$ in EC/DMC with 1/1 volume ratio)

(22) Lanz, M.; Kormann, C.; Steininger, H.; Heil, G.; Haas, O.; Novak, P. *J. Electrochem. Soc.* **2000**, *147*, 3997.

(23) Wang, X.; Tanaike, O.; Kodama, M.; Hatpri, H. *J. Power Sources* **2007**, *168*, 282.

(24) Chiu, K. F.; Lin, H. C.; Lin, K. M.; Chen, C. C. *J. Electrochem. Soc.* **2006**, *153*, A1992.

(25) (a) Blyr, A.; Sigala, C.; Amatucci, G.; Guyomard, D.; Chabre, Y.; Tarascon, J. M. *J. Electrochem. Soc.* **1998**, *145*, 194. (b) Sun, Y. K.; Yoon, C. S.; Kim, C. K.; Youn, S. G.; Lee, Y. S.; Yoshio, M.; Oh, I. H. *J. Mater. Chem.* **2001**, *11*, 2519.

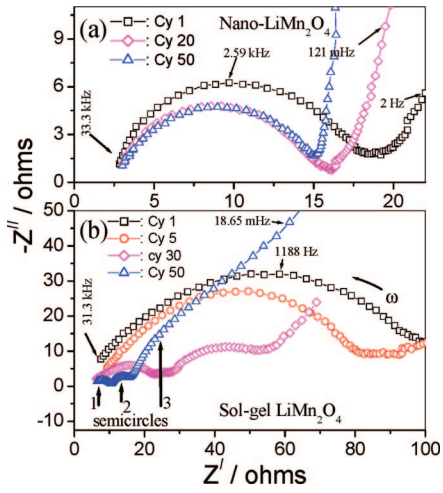

Figure 6. Complex impedance plots at the end of discharge for (a) nano- and (b) sol−gel LiM_2O_4. Plots for select cycles.

was determined for nano- and sol−gel $LiMn_2O_4$. Equal masses (100 mg) of nano-$LiMn_2O_4$ and sol−gel $LiMn_2O_4$ were immersed in 5 mL of LP30 electrolyte at 30 °C, and the manganese content in the solution was determined after 1 and 2 days of exposure. The measured manganese contents after 1 day were 33 (24) and 75 (58) ppm, respectively, for the nano- and sol−gel $LiMn_2O_4$, with the values in the parentheses representing the dissolution normalized per unit area of the material. The respective values after 2 days of exposure to the electrolyte were 37 (27) and 97 (75) ppm. The dissolution at 50 °C was also determined, and the respective manganese contents after 30 days of exposure were 98 (70) and 248 (191) ppm. Evidently, nano-$LiMn_2O_4$ is less soluble than sol−gel $LiMn_2O_4$ at 30 and 50 °C.

Dissolution occurs at the electrode/electrolyte interface. The lower solubility and superior structural stability of nano-$LiMn_2O_4$ signals a more stable interface. Alternating current impedance has been used to study the electrolyte/spinel interface.[26−28] It is used here to study nano- and sol−gel $LiMn_2O_4$. All data were collected on three-electrode cells and therefore relate only to the response of the spinel electrodes. The ac impedance data after various numbers of cycles are shown in Figure 6. Comparing the results for nano- and sol−gel $LiMn_2O_4$, the ac impedance for the former is lower than the latter and varies much less on cycling. Throughout the cycling range, nano-$LiMn_2O_4$ exhibits a single semicircle, which may be described by a combination of a resistance, capacitance, and constant phase element (CPE). Nonlinear least-squares fitting reveals that this semicircle is associated with a capacitance of ~40 μF cm^{-2}. On cycling, the impedance reduces by only a few ohms and the capacitance remains invariant. These results are consistent with a very stable interface. This behavior is in contrast to that observed for sol−gel $LiMn_2O_4$, where there are significant changes in the impedance on cycling, with the development of 2−3 semicircles, Figure 6b. The high-frequency semicircle at cycle 50 is associated with a capacitance of 120 μF cm^{-2}. The second (intermediate frequency) semicircle at cycle 50 is associated with a capacitance of approximately 3 mF cm^{-2} and the low-frequency semicircle with ~35 mF cm^{-2}. Such high capacitances have been noted before and are indicative of processes directly on the electrode surface.[26,28] The invariance of ac impedance on cycling nano-$LiMn_2O_4$ compared with sol−gel $LiMn_2O_4$ is consistent with the superior structural stability and capacity retention of the former.

What then is the origin of the stable cycling, good rate capability, excellent structural stability, and invariant ac impedance of nano-$LiMn_2O_4$, when stoichiometric $LiMn_2O_4$, in general, whether composed of micrometer or nanometer particles, does not exhibit such behavior? Could it be related to differences in the formation of the SEI layer that is expected to form on the surface of $LiMn_2O_4$ when in contact with the electrolyte?[26,29] Given the results discussed above, especially, the similarity in capacity retention of nano-$LiMn_2O_4$ and surface-coated stoichiometric spinels, Table 1, it is possible that the nano-$LiMn_2O_4$ particles become coated with a protective layer during synthesis. However, high-resolution TEM failed to provide any clear evidence of a surface layer on as-prepared nano-$LiMn_2O_4$ particles, Figure 2 and the CHN analysis supported the absence of any residual carbon from pyrolysis of the organics in air, as expected. The surface/near-surface region appears very similar to other uncoated particles, e.g., sol−gel $LiMn_2O_4$, Figure 2. If a separate surface layer exists, it must be very thin. X-ray photoelectron spectroscopy (XPS) studies also failed to identify the presence of a foreign surface on the nano-$LiMn_2O_4$ particles. However, more detailed studies, including XPS with depth profiling, are underway to investigate the surface further, especially whether the synthesis conditions modify the surface composition or surface structure of spinel in a fashion that could account for the enhanced stability.

Conclusion

In conclusion, stoichiometric $LiMn_2O_4$ spinel has been synthesized with a morphology composed of nanoparticles (50−100 nm) fused to form a porous structure, which is retained on electrode fabrication and cycling. The material exhibits a high initial capacity (131 mA·h g^{-1}) and retains 118 mA·h g^{-1} after 200 cycles, at a discharge rate of *C*/2. It also exhibits excellent rate capability, retaining

(26) (a) Aurbach, D.; Markovsky, B.; Levi, M. D.; Levi, E.; Schechter, A.; Moshkovich, M.; Cohen, Y. *J. Power Sources* **1999**, *81*−*82*, 95. (b) Aurbach, D.; Gamolsky, K.; Markovsky, B.; Salitra, G.; Gofer, Y.; Heider, U.; Oesten, R.; Schmidt, M. *J. Electrochem. Soc.* **2000**, *147*, 1322.
(27) (a) Mohamedi, M.; Takahashi, D.; Uchiyama, T.; Itoh, T.; Nishizawa, M.; Uchida, I. *J. Power Sources* **2001**, *93*, 93. (b) Shaju, K. M.; Subba Rao, G. V.; Chowdari, B. V. R. *J. Mater. Chem.* **2003**, *13*, 106. (c) Dokko, K.; Mohamedi, M.; Umeda, M.; Uchida, I. *J. Electrochem. Soc.* **2003**, *150*, A425.
(28) (a) Thomas, M. G. S. R.; Bruce, P. G.; Goodenough, J. B. *J. Electrochem. Soc.* **1985**, *132*, 1521. (b) Conway, B. E. *J. Electrochem. Soc.* **1991**, *138*, 1539. (c) Choi, Y. M.; Pyun, S. I.; Bae, J. S.; Moon, S. I. *J. Power Sources* **1995**, *56*, 25.
(29) (a) Edstrom, K.; Gustafsson, T.; Thomas, J. O. *Electrochim. Acta* **2004**, *50*, 397. (b) Eriksson, T.; Gustafsson, T.; Thomas, J. O. *Electrochem. Solid-State Lett.* **2002**, *5*, A35.
(30) Tronel, F.; Guerlou-Demourgues, L.; Menetrier, M.; Croguennec, L.; Goubault, L.; Bernard, P.; Delmas, C. *Chem. Mater.* **2006**, *18*, 5840.

90% of its capacity at 40*C* and 85% at 60*C*. Cycling at a rate of 10*C* is associated with nearly 100% power retention (5840 W kg^{-1} (of $LiMn_2O_4$) dropping to 5828 W kg^{-1} after 1000 cycles). Volumetric energy density, at 10*C*, based on the total volume of the composite electrode, is $\sim$750 W·h L^{-1}. Capacity retention is superior to stoichiometric $LiMn_2O_4$ with a similar surface area. Differences in the capacity retention on cycling are reflected in superior structural stability, lower Mn dissolution, and relatively invariant ac impedance of nano-$LiMn_2O_4$ compared with sol−gel $LiMn_2O_4$, results that suggest nano-$LiMn_2O_4$ particles may possess a stabilized surface that inhibits dissolution.

Acknowledgment. P.G.B. is indebted to the EPSRC including the SUPERGEN program and EU for financial support.

CM8010925